Heteroatom Chemistry
Volume 25, Number 6, 2014

# N,S,P-Hybrid Donor–$\pi$–Acceptor Organic Dyes for Dye-Sensitized Solar Cell: Synthesis, Optical Properties, and Photovoltaic Performances

Yoshihiro Matano,[1] Yukiko Hayashi,[2] Haruyuki Nakano,[3] and Hiroshi Imahori[2,4]

[1]*Department of Chemistry, Faculty of Science, Niigata University, Niigata 950-2181, Japan*

[2]*Department of Molecular Engineering, Graduate School of Engineering, Kyoto University, Kyoto 615-8510, Japan*

[3]*Department of Chemistry, Graduate School of Sciences, Kyushu University, Fukuoka 812-8581, Japan*

[4]*Institute for Integrated Cell-Material Sciences (WPI-iCeMS), Kyoto University, Kyoto 615-8510, Japan*

*Received 15 February 2014; revised 3 May 2014*

ABSTRACT: *New donor–π–acceptor organic (D–π–A) dyes composed of triarylamine, oligothiophene, and phosphole subunits were prepared, and their optical and photovoltaic properties were investigated. The regioselective α-lithiation of the thiophene ring of 2-(thiophen-2-yl)phospholes bearing an ester group, followed by treatment with tributyltin chloride afforded 2-(5-(tributylstannyl)thiophen-2-yl)phosphole derivatives, which underwent Stille coupling with 5′-(p-(diarylamino)phenyl)-5-bromo-2,2′-bithiophene to give triarylamine–terthiophene–phosphole hybrid π systems bearing the terminal ester group. The alkaline hydrolysis of the ester group yielded the target dyes, bearing the carboxylic acid anchoring group. The UV–vis absorption spectra of the new N,S,P-hybrid dyes displayed broad and intense π–π* transitions with two absorption maxima in the visible region. Density functional theory (DFT) calculations of two dye models revealed that each highest occupied molecular orbital (HOMO) resides on the triarylamine–oligothiophene π network, whereas each lowest unoccupied molecular orbital (LUMO) is basically located on the phosphole subunit. In addition, the time-dependent DFT calculations of the models showed that the lowest energy bands of these hybrid dyes are mainly consisted of the HOMO-to-LUMO+1 and HOMO-to-LUMO transitions with the large intramolecular charge-transfer character. The N,S,P-hybrid-dye-sensitized $TiO_2$ cells exhibited moderate power conversion efficiencies of up to 5.6%. The present findings corroborate the potential utility of the phosphole skeletons as the acceptor components in the D–π–A sensitizers.* © 2014 Wiley Periodicals, Inc. Heteroatom Chem. 25:533–547, 2014; View this article online at wileyonlinelibrary.com. DOI 10.1002/hc.21188

*Correspondence to*: Yoshihiro Matano; e-mail: matano@chem.sc.niigata-u.ac.jp.

Dedicated to Professor Renji Okazaki on the occasion of his 77th birthday.

Contract grant sponsor: Grants-in-Aid from the Ministry of Education, Culture, Sports, Science and Technology, Japan. Contract grant number: 25288020. Contract grant sponsor: Ogasawara Foundation.

## *INTRODUCTION*

Inspired by the Grätzel's pioneering work on dye-sensitized solar cells (DSSCs) with mesoporous $TiO_2$ [1], a variety of organic dyes have been designed and synthesized for uses in DSSCs. Among them, the most extensively investigated are ruthenium–polypyridine complexes, which efficiently utilize the metal-to-ligand charge transfer (MLCT) transitions for harvesting a wide range of visible and near-infrared (vis/NIR) light [2]. Recent advances in this research area have also been led by a new class of organic sensitizers that do not rely on the ruthenium-assisted MLCT. In particular, metal-free or inexpensive metal-incorporated donor–$\pi$–acceptor type organic-based dyes (D–$\pi$–A dyes) bearing the anchoring group at the terminal acceptor unit have received increasing attention [3], because the separation of D and A units is likely to induce (i) the large charge-transfer (CT) character for the $\pi$–$\pi^*$ transitions, resulting in the high light–harvesting ability in the vis/NIR region, (ii) the efficient electron injection from the excited dye to a conduction band (CB) of $TiO_2$ electrode through the acceptor unit, and (iii) the suppression of the fast charge recombination between the injected electrons and the dye radical cation.

To date, various kinds of D–$\pi$–A dyes have been examined, among which the amine–oligothiophene–acceptor $\pi$ frameworks have proven to be effective for the achievement of high cell performances [4]. For example, MK-2-modified and C217-modified $TiO_2$ DSSCs exhibited high $\eta$ values up to 8.3% [4c] and 9.9% [4e], respectively (Chart 1). To further improve the cell performances, however, it is necessary to enhance the light-harvesting ability in the longer wavelength region. In this regard, the fine-tuning of the highest occupied molecular orbital and lowest unoccupied molecular orbital (HOMO–LUMO) gap of the D–$\pi$–A dyes by chemical modification is still an important subject.

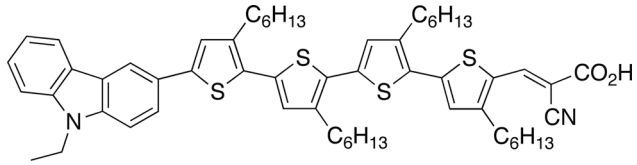


**MK2**

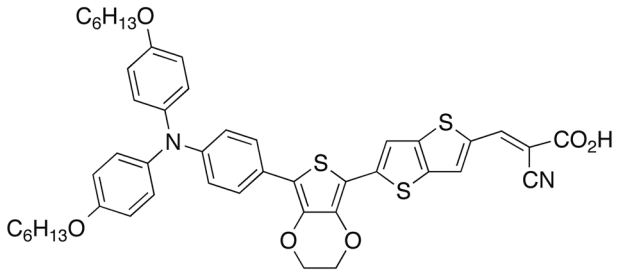


**C217**

**CHART 1**

Phosphole, a phosphorus-bridged cyclic 1,3-diene, is a promising constituent for making $\pi$-conjugated organic materials with a low-lying LUMO, a narrow HOMO–LUMO gap, and a polarizable $\pi$ spacer [5]. These characteristic properties of phosphole are derived from the effective $\sigma^*$–$\pi^*$ orbital interaction between the phosphorus center and the adjacent 1,3-diene unit. In addition, chemical functionalizations at the phosphorus atom change the optoelectronic properties of phosphole-containing $\pi$-systems significantly. For instance, the P-thioxidation enhances the electron-accepting and electron-transporting abilities of the phosphole-based fused $\pi$ systems [6]. We have recently reported a series of $\pi$-conjugated phosphole–arene [7], phosphole–vinylene [8] and phosphole–acetylene [9] derivatives by using titanacycle-mediated metathesis and cross-coupling reactions [10]. Such phosphole-containing hybrid $\pi$-systems have exhibited the intrinsic D–A character in their excited states, as the phosphole ring behaves as the highly electron-accepting and polarizable unit as mentioned above. For instance, thiophene–phosphole–vinylene $\pi$ systems bearing the electron-donating substituents at the terminal thiophene ring showed redshifted absorption/emission bands, large Stokes shifts, and large hyperpolarizability compared to the unsubstituted reference. These results suggested to us that the donor–thiophene–phosphole $\pi$ system would be utilized for the construction of D–$\pi$–A sensitizers [11].

We report herein the first examples of triarylamine–oligothiophene–phosphole derivatives as a new class of D–$\pi$–A dyes for use in DSSC. The target dyes were prepared by using the titanacycle-mediated metathesis and Stille coupling reactions as key steps. We also elucidated the optical and electrochemical properties of the new dyes and applied them to DSSC. The effects of the vinylene and phenylene bridges on the power conversion efficiencies will be discussed.

## *RESULTS AND DISCUSSION*

### *Synthesis*

Schemes 1 and 2 illustrate the syntheses of new D–$\pi$–A dyes **7** and **12**, respectively. Sonogashira coupling of 1-(thiophene-2-yl)hepta-1,6-diyne [8a] with (*E*)-ethyl 3-iodoacrylate gave difunctionalized

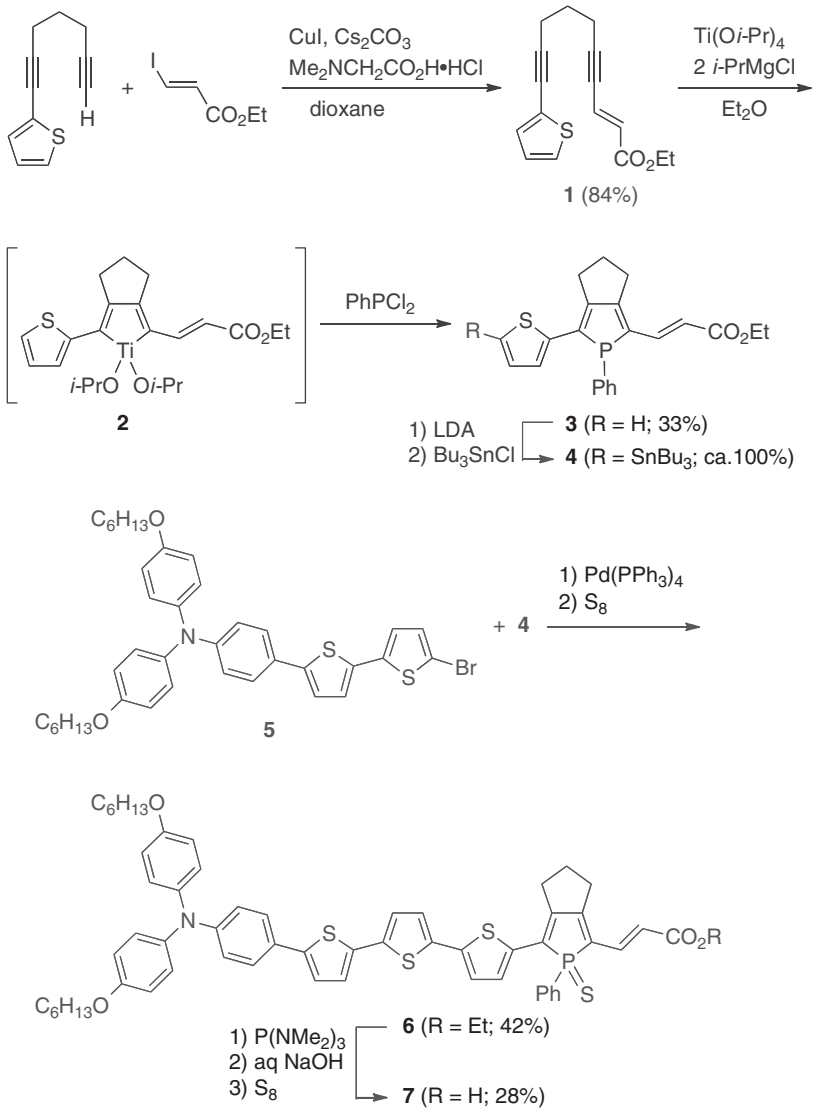


**SCHEME 1** Synthesis of **7**.

enediyne **1**. Treatment of **1** with a low valent titanium reagent, generated from Ti(O*i*-Pr)$_4$ and *i*-PrMgCl [12], gave $\alpha$,$\alpha$'-difunctionalized titanacycle **2**, which underwent a metathesis reaction with dichloro(phenyl)phosphine to afford 2-(thiophen-2-yl)-5-(2-(ethoxycarbonyl)ethenyl)phosphole **3** in 33% yield based on **1**. The ortho-lithiation of the thiophene ring of **3** with lithium diisopropylamide (LDA) followed by addition of tributyltin chloride produced the $\alpha$-tributylstannyl derivative **4** as a pale brown oil, which was used without further purification for the subsequent Stille coupling reaction. The palladium-catalyzed Stille coupling of **4** with triarylamine-appended 5-bromo-2,2'-bithiophene **5** proceeded at reflux in toluene, affording the triarylamine–terthiophene–phosphole hybrid $\pi$ system **6** after sulfrization. Compound **6** was purified by silica-gel column chromatography and isolated as a reddish black solid in 42% yield. Attempts to hydrolyze the ester group of **6** under basic conditions resulted in partial degradation of the phosphole unit, probably due to the involvement of the P=S function. Therefore, we removed the sulfur protection from the phosphorus center during the course of hydrolysis. Desulfrization of the $\sigma^4$-P=S ester **6** with P(NMe$_2$)$_3$ proceeded smoothly to give the $\sigma^3$-P ester ($R_f$ = 0.65, hexane/EtOAc = 3:1), which was subsequently treated with the aqueous NaOH solution in THF–EtOH. The hydrolysis of the ester function was complete within 24 h at 45°C, and the resulting $\sigma^3$-P carboxylic acid ($R_f$ = 0.33, hexane/EtOAc = 3/1) was converted to the $\sigma^4$-P=S carboxylic acid **7** by adding elemental sulfur. After silica-gel column chromatography, the target dye **7** was

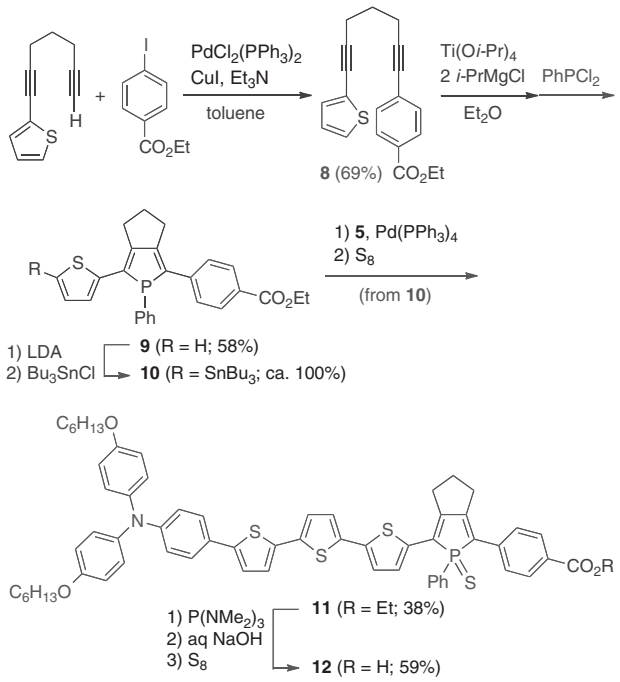


**SCHEME 2** Synthesis of **12**.

isolated in 28% yield (based on **6**) as a reddish black solid.

The N,S,P-hybrid dye **12** was prepared starting from **8** via **9**–**11**, according to the similar procedures employed for the synthesis of **7**. The isolated new compounds were fully characterized by conventional spectroscopic techniques ($^1$H NMR, $^{31}$P NMR, IR, and high-resolution MS).

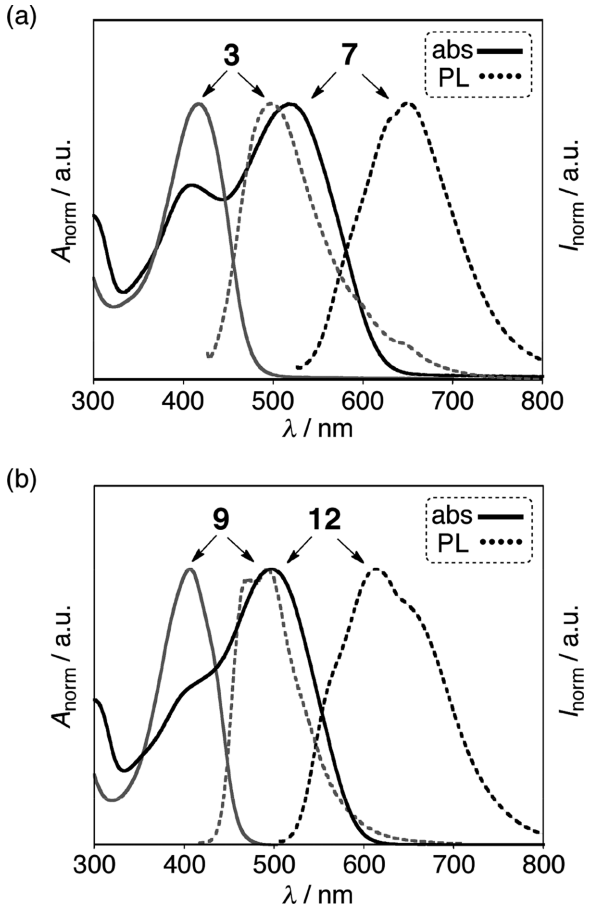


**FIGURE 1** UV–vis absorption (solid line) and fluorescence (dashed line) spectra of (a) **3**, **7** and (b) **9**, **12** in toluene. The excitation wavelengths are 417 nm for **3**, 517 nm for **7**, 407 nm for **9**, and 497 nm for **12**. All the spectra are normalized for comparison.

## *Optical and Electrochemical Properties*

The optical properties of **3**, **7**, **9**, and **12** were investigated by using UV–vis absorption/fluorescence spectroscopy. As shown in Fig. 1 and Table 1, the reference dye **3** displayed broad and intense $\pi$–$\pi^*$ transitions with the absorption and emission maxima at $\lambda_{abs} = 417$ and $\lambda_{em} = 497$ nm, respectively, in toluene. On the other hand, the N,S,P-hybrid dye **7** exhibited two intense absorption bands in the visible region (see below). The attachment of the electron-donating triarylamine unit and the P-sulfrization (from **3** to **7**) induces the large redshifts of the absorption and emission maxima ($\lambda_{abs} = 517$ and $\lambda_{em} = 649$ nm), implying that the CT character is largely enhanced through the elongated $\pi$ network in **7**. The same trend was observed for the phenylene-bridged derivatives **9** ($\lambda_{abs} = 407$ and $\lambda_{em} = 469$, 494 nm) and **12** ($\lambda_{abs} = 497$ and $\lambda_{em} = 614$ nm). From the intersection of the normalized absorption and emission spectra, the zero–zero excitation energy ($E_{0-0}$) values of **7** and **12** were determined to be 2.13 and 2.23 eV, respectively. The change from the vinylene to the phenylene bridge (from **7** to **12**) on the anchoring group causes slight blueshifts of both the $\lambda_{abs}$ and $\lambda_{em}$ values (see below).

Redox potentials of **3**, **7**, **9**, and **12** were measured in $CH_2Cl_2$ by using cyclic voltammetry (CV) and differential pulse voltammetry (DPV) with 0.1 M $n$Bu$_4$NPF$_6$ as a supporting electrolyte (for details, see the Experimental section). The reference dyes **3** and **9** showed an irreversible oxidation process in CV measurements, and the oxidation potentials ($E_{ox}$) were determined by DPV to be +0.66 V (for **3**) and +0.59 V (for **9**) versus ferrocene/ferrocenium (Fc/Fc$^+$). By contrast, the N,S,P-hybrid dyes **7** and **12** displayed two reversible oxidation processes, and their first and second oxidation potentials ($E_{ox,1}$ and $E_{ox,2}$) were determined to be +0.19 and +0.47 V for **7** and +0.18 and +0.44 V for **12** versus Fc/Fc$^+$. It is apparent that the $\alpha$-substitution of the thiophene

**TABLE 1** Optical and Electrochemical Data for **3**, **7**, **9**, and **12** and Driving Forces for Electron Transfer Processes on $TiO_2$ for **7** and **12**

| *Dye* | $\lambda_{abs}$ *(nm)*[a] *(log* $\varepsilon$*)* | $\lambda_{em}$ *(nm)*[b] | $E_{ox,1}$ *(V)*[c] | $E_{red}$ *(V)*[c] | $E_{0-0}$ *(eV)* | $E_{ox}$* *(V)*[d] | $\Delta G_{inj}$ *(eV)*[e] | $\Delta G_{reg}$ *(eV)*[f] |
|---|---|---|---|---|---|---|---|---|
| **3** | 417 (4.09) | 497 | +1.30 | –1.39 | 2.71 | – | – | – |
| **7** | 517 (4.57) | 649 | +0.83 | –1.21 | 2.13 | –1.30 | –0.80 | –0.43 |
| **9** | 407 (4.22) | 469, 494 | +1.23 | n. d.[g] | 2.85 | – | – | – |
| **12** | 497 (4.85) | 614 | +0.82 | –1.29 | 2.23 | –1.41 | –0.91 | –0.42 |

[a]Absorption maxima in toluene.
[b]Emission maxima in toluene by exciting at 417 nm for **3**, 517 nm for **7**, 407 nm for **9**, and 497 nm for **12**.
[c]Ground state oxidation ($E_{ox}$) and reduction ($E_{red}$) potentials (vs. NHE).
[d]Excited-state oxidation potentials approximated from $E_{ox}$ and $E_{0-0}$ (vs. NHE).
[e]Driving forces for electron injection from the dye singlet excited state ($E_{ox}$*) to the CB of $TiO_2$ (–0.5 V vs. NHE).
[f]Driving forces for the regeneration of the dye radical cation ($E_{ox}$) by the $I^-/I_{3-}$ redox couple (+0.4 V vs. NHE).
[g]n. d. = Not determined.

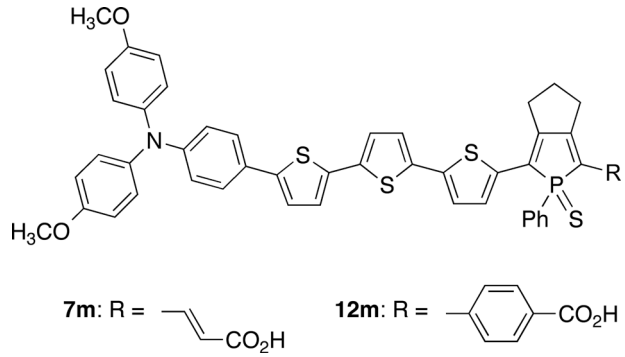


**CHART 2**

ring with the *p*-(diarylamino)phenyl group stabilizes the electrochemically oxidized states and raises the HOMO levels of the entire $\pi$ systems.

## *Theoretical Calculations*

To get some insights into the electronic structures of the D–$\pi$–A dyes **7** and **12**, we performed density functional theory (DFT) calculations on their models **7m** and **12m** at the B3LYP/6-31G(d,p) level including the solvent effect of toluene (Chart 2). At the optimized structures of **7m** and **12m**, the aniline, terthiophene, and phosphole rings are coplanar with the torsion angles at the interring bonds of 3–20°, implying that these D–$\pi$–A components are effectively $\pi$ conjugated. Figure 2 summarizes the Kohn–Sham orbitals of HOMO–2, HOMO–1, HOMO, LUMO, and LUMO+1 together with their energies. It is obvious that the orbital coefficients of HOMO are located at the triarylamine–terthiophene moieties, whereas those of LUMO are mainly at the phosphole–anchoring groups and to a small extent at the neighboring thiophene ring. On the other hand, HOMO–2, HOMO—1, and LUMO+1 are spread over the entire $\pi$ system compared to the HOMO and LUMO. The HOMO levels of **7m** and **12m** are close to each other, which is in good agreement with a small difference in the oxidation potentials between **7** and **12**. By contrast, the LUMO level of **7m** is considerably stabilized compared to that of **12m**, which stems from the different geometry at the phosphole–anchoring groups. Thus, the phosphole and vinylene units in **7m** are almost on the same plane (dihedral angle = 7°), whereas the phosphole and phenylene units in **12m** are appreciably twisted (dihedral angle = 42°). This implies that the $\pi$ conjugation in **7** is more effective than that in **12** (see below).

With the optimized structures in hand, we next performed the time-dependent density functional theory (TD-DFT) calculations on **7m** and **12m** with the long-range corrected Becke–Lee–Yang–Parr (LC-BLYP) exchange-correlation functional including the solvent effect of toluene. As shown in Table 2, two intense $\pi$–$\pi$* transitions were calculated for each chromophore: The lower energy bands ($\lambda$ = 461 nm for **7m** and 430 nm for **12m**) are mainly composed of the HOMO-to-LUMO and HOMO–1-to-LUMO transitions, whereas the higher energy bands ($\lambda$ = 372 nm for **7m** and 357 nm for **12m**) are composed of the HOMO-to-LUMO+1 and HOMO–2-to-LUMO transitions. These LC-BLYP calculations qualitatively support the two split bands observed for **7** and **12**. It is evident that the HOMO-to-LUMO transition includes the large CT character from the donor (triarylamine–thiophene) to the acceptor (phosphole–anchoring group) units. In this regard, the lowest excited states in **7m** and **12m** essentially possess the large CT character. The HOMO–1-to-LUMO transition also includes the moderate CT character. These results imply that the present molecular design, namely, the incorporation of phosphole as the acceptor unit, is promising for the construction of the polarizable D–$\pi$–A structure. The lowest excitation energy of **7m** is smaller than that of **12m**, which agrees well with the observed results and explains the difference in their $\pi$ conjugation (see above).

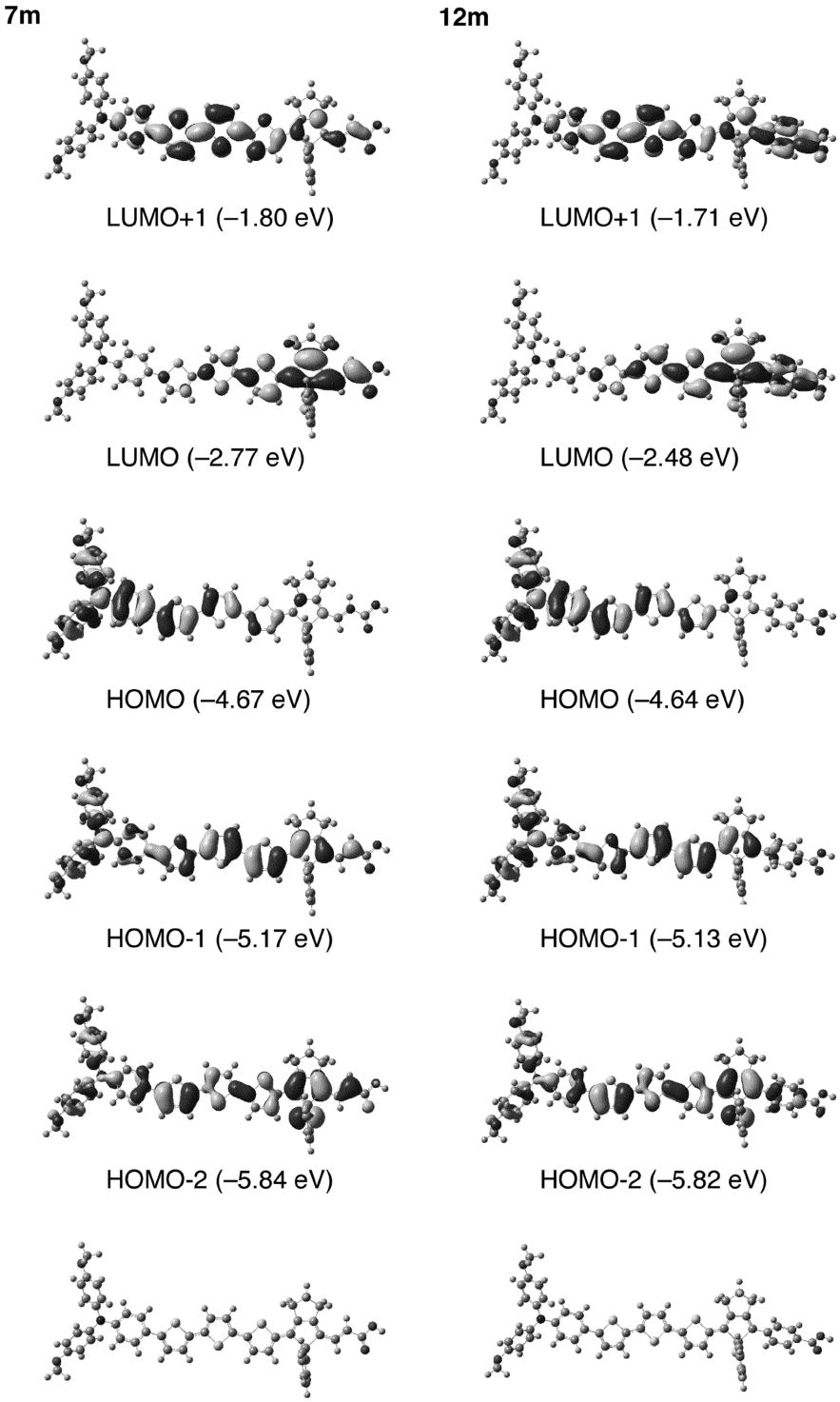


**FIGURE 2** Kohn–Sham orabitals: HOMO–2, HOMO–1, HOMO, LUMO, and LUMO+1 of (a) **7m** and (b) **12m** and their energies calculated by the DFT method [B3LYP/6-31G(d,p)]. The optimized structures are shown at the bottom.

### *Photovoltaic Properties of New D–π–A-Dye-Sensitized $TiO_2$ Cells*

With the $E_{ox,1}$ values of 0.83 V versus normal hydrogen electrode (NHE) (0.19 V vs. $Fc/Fc^+$) and the $E_{0-0}$ values of 2.13 eV for **7**, driving forces for the electron injection from the dye-excited state to the CB of $TiO_2$ (–0.5 V vs. NHE) [13] ($\Delta G_{inj}$) and the regeneration of the dye radical cation by the $I^-/I_3^-$ redox couple (+0.4 V vs. NHE) ($\Delta G_{reg}$) for the **7**-sensitized

solar cell were evaluated to be –0.80 and –0.43 eV, respectively (Table 1 and Scheme 3). Similarly, the $\Delta G_{inj}$ and $\Delta G_{reg}$ values for the **12**-sensitized solar cell were –0.91 and –0.42 eV, respectively. Therefore, both processes are thermodynamically feasible for **7** and **12** [14].

Considering these energy diagrams, we evaluated cell performances for $TiO_2$/**7** cells under various adsorption conditions. First, the $TiO_2$ electrodes were modified with **7** by immersing $TiO_2$ electrodes into toluene solutions of **7** (0.3 mM) for 1–12 h. The resulting dye-adsorbed $TiO_2$ cells were measured under AM 1.5 under simulated solar light (100 mW $cm^{-2}$) in the presence of electrolyte (0.1 M LiI, 0.03 M $I_2$), 2,3-dimethyl-1-propylimidazolium iodide (0.6 M), and *tert*-butylpyridine (0.5 M) in acetonitrile–valeronitrile (for details, see the Experimental section). The power conversion efficiency ($\eta$) is derived from the equation $\eta = J_{SC} \times V_{OC} \times ff$, where $J_{SC}$ is the short circuit current, $V_{OC}$ is the open circuit potential, and *ff* is the fill factor. The $\eta$ values of the $TiO_2$/**7** cell reached 3.1% after 1 h and did not show a significant dependence on the immersion time (Fig. 3, entry 1 in Table 3). Presumably, the substituents around the phosphorus atom of **7** as well as the bent structure of the entire D–$\pi$–A $\pi$ system suppress the dye aggregation after the initial adsorption onto the $TiO_2$ surface. Indeed, addition of chenodeoxycholic acid did not improve the $\eta$ value. To further optimize the cell performances, we examined the effects of the solvent and the concentration of $I_2$ in the range of 0.03–0.15 M (entries 2–4). The use of acetonitrile gave the better result ($\eta$ = 3.4%) than that of an acetonitrile/valeronitrile mixed solvent. When 0.06 M of $I_2$ was used, the $J_{SC}$ and $\eta$ values increased slightly (entry 3 in Table 3 and Fig. 4). Under the optimized conditions (immersed for 8 h in acetonitrile, measured with 0.06 M of $I_2$), the $TiO_2$/**12** cell exhibited the $\eta$ value of 5.6% (entry 5 in Table 3 and Fig. 4). To our knowledge, this is the highest $\eta$ value ever reported for the phosphole-containing DSSCs. We have previously reported two dithieno[2,3-b:3′,2′-d]phosphole-based dyes for DSSC, in which the $R_2P(O)OH$ group was used as the anchor [11].

The $\eta$ value of the $TiO_2$/**12** cell (5.6%) is considerably higher than that of the $TiO_2$/**7** cell (3.7%). As the $V_{OC}$ and *ff* values in these two cells are largely similar, the increase in $\eta$ values mainly stems from the increase in $J_{SC}$ values. As shown in Figs. 5 and 6, the photocurrent action spectra of these cells basically reflect the absorption spectra of **7** and **12** adsorbed on the electrodes, indicating that the photocurrents are generated from the sensitized **7** and **12**. The incident photon-to-current efficiency (IPCE)

**TABLE 2** Excitation energies (<3.9 eV) and oscillator strengths of **7m** and **12m** calculated by the TD-DFT method with the LC-BLYP functional and solvent effect (PCM, toluene)[a]

| State | Excitation Energy (eV) | Excitation Energy (nm) | Oscillator Strength | Excitation | Weight (%) |
|---|---|---|---|---|---|
| **7m** | | | | | |
| 1 | 2.68 | 462 | 1.909 | HOMO → LUMO | 27.4 |
| | | | | HOMO–1 → LUMO | 42.5 |
| 2 | 3.33 | 372 | 0.401 | HOMO → LUMO+1 | 40.5 |
| | | | | HOMO–2 → LUMO | 21.1 |
| **12m** | | | | | |
| 1 | 2.88 | 431 | 2.068 | HOMO → LUMO | 33.0 |
| | | | | HOMO–1 → LUMO | 37.9 |
| 2 | 3.47 | 357 | 0.192 | HOMO → LUMO+1 | 33.0 |
| | | | | HOMO–2 → LUMO | 24.0 |

[a]The excitations whose weights are less than 15% are not included.

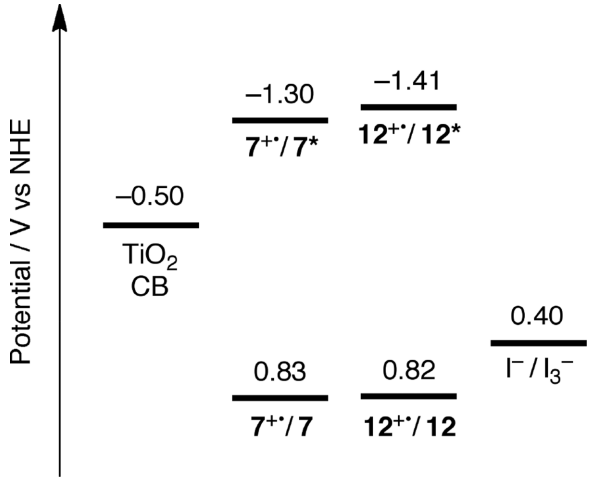


**SCHEME 3** Energy diagrams for DSSCs of **7** and **12**.

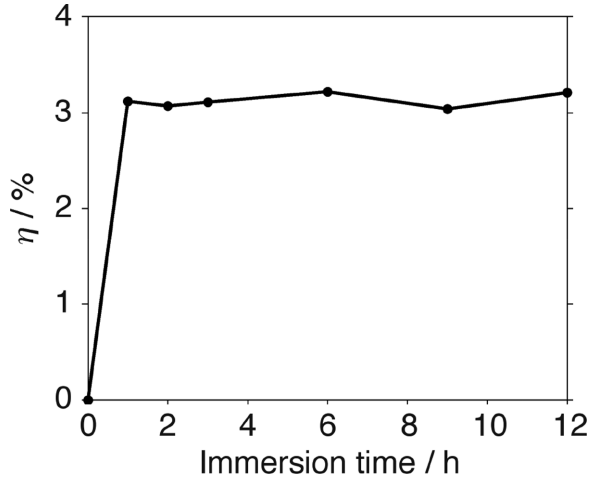


**FIGURE 3** Immersion time profile of the $\eta$ values of the $TiO_2$/**7** cell. The dye **7** was adsorbed onto the $TiO_2$ electrodes by immersing $TiO_2$ electrodes into MeCN/valeronitrile (85:15) solutions of **7**.

**TABLE 3** Photovoltaic Data for DSSCs[a]

| Entry | Cell [Immersion Time (h)] | $[I_2]$ (M) | $J_{SC}$ (mA $cm^{-2}$) | $V_{OC}$ (V) | *ff* | $\eta$ (%) |
|---|---|---|---|---|---|---|
| 1 | $TiO_2$/**7** (3) | 0.03 | 7.6 | 0.60 | 0.68 | 3.1 |
| 2 | $TiO_2$/**7** (3) | 0.03 | 8.1 | 0.61 | 0.69 | 3.4 |
| 3 | $TiO_2$/**7** (3) | 0.06 | 9.0 | 0.61 | 0.68 | 3.7 |
| 4 | $TiO_2$/**7** (3) | 0.15 | 8.2 | 0.59 | 0.70 | 3.4 |
| 5 | $TiO_2$/**12** (8) | 0.06 | 12.5 | 0.63 | 0.70 | 5.6 |

[a]Entry 1: in MeCN/valeronitrile = 85/15. Entries 2–5: in MeCN.

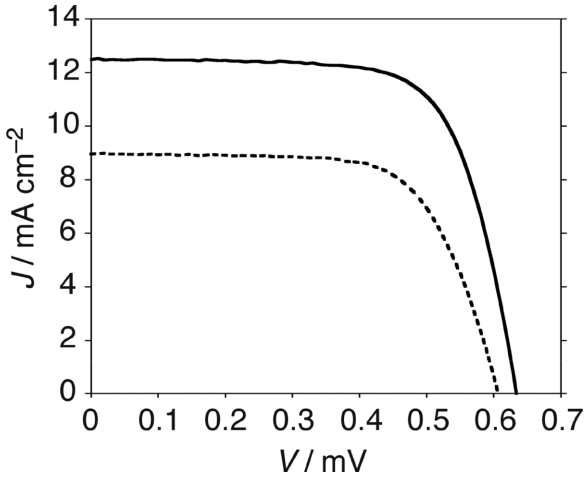


**FIGURE 4** Photocurrent–voltage characteristics of the $TiO_2$/**7** cell (dashed line; $\eta = 3.7$, $J_{SC} = 9.0$, $V_{OC} = 0.61$, $ff = 0.68$) and the $TiO_2$/**12** cell (solid line; $\eta = 5.6$, $J_{SC} = 12.5$, $V_{OC} = 0.63$, $ff = 0.70$). Conditions: electrolyte, 0.1 M LiI, 0.05 M $I_2$, 0.6 M 2,3-dimethyl-1-propylimidazolium iodide, and 0.5 M *tert*-butylpyridine in MeCN; input power, AM 1.5 under simulated solar light (100 mW $cm^{-2}$). $\eta = J_{SC} \times V_{OC} \times ff$.

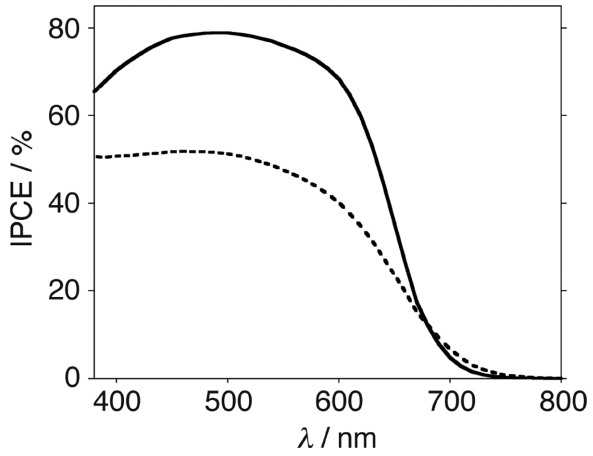


**FIGURE 5** Photocurrent action spectra of the $TiO_2$/**7** cell (dashed line) and the $TiO_2$/**12** cell (solid line).

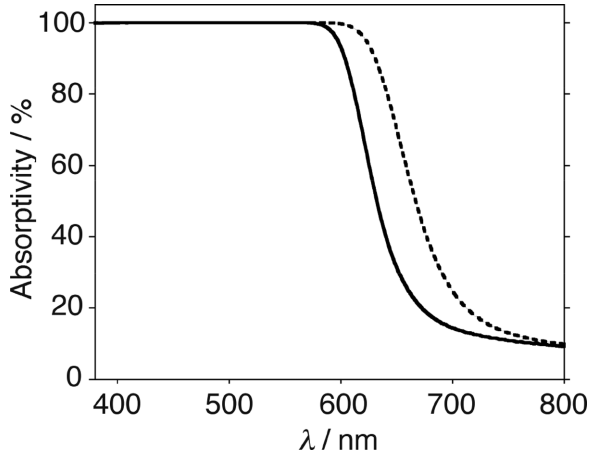


**FIGURE 6** Absorption spectra of the $TiO_2$/**7** electrode (dashed line) and the $TiO_2$/**12** electrode (solid line). The scattering $TiO_2$ layers were not applied to the $TiO_2$ electrodes to measure absorbance accuracy.

is divided into three components in the following equation:

$$\mathrm{IPCE} = \mathrm{LHE} \times \phi_{\mathrm{inj}} \eta_{\mathrm{col}} \quad (1)$$

where LHE (light-harvesting efficiency) is the number of absorbed photons per the number of incident photons, $\phi_{\mathrm{inj}}$ is the quantum yield for electron injection from the dye-excited singlet state to the CB of the $TiO_2$ electrode, and $\eta_{\mathrm{col}}$ is the efficiency of charge collection. The maximal IPCE values for the $TiO_2$/**7** (52%) and $TiO_2$/**12** (79%) cells were observed at ca. 460 and 490–500 nm, respectively, which largely correspond to the absorption maxima of **7** and **12** in toluene. The $TiO_2$/**7** cell displays the lower IPCE values than the $TiO_2$/**12** cell in most of the visible region (Fig. 5). On the other hand, the LHE values of the $TiO_2$/**7** cell are comparable to (380–600 nm) or even higher than (>600 nm) those of the $TiO_2$/**12** cell (Fig. 6). These data suggest that the markedly different IPCE values are attributed to the lower electron injection and/or charge collection efficiencies of the $TiO_2$/**7** cell than those of the $TiO_2$/**12** cell. The DFT calculations of the models **7m** and **12m** show the sufficient orbital coefficients at the anchoring carboxylic acid group in each LUMO together with no aggregation effect of the dyes on $TiO_2$, suggesting that the electron injection efficiencies of the dyes **7** and **12** are comparable. Considering these factors, we can conclude that the charge collection efficiency of **7** is lower than that of **12**. It is known that the charge collection efficiency of DSSCs is affected by charge recombination between the injected electron in the CB of the $TiO_2$ electrode and the dye radical cation and/or $I_3^-$ in the electrolyte solution [2–4]. Specifically, the former process is governed by the separation distance and geometry between the dye core and the $TiO_2$ surface: The shorter the distance is the faster the charge

recombination from the electrons in the CB of $TiO_2$ to the dye radical cation takes place [15]. It has also been revealed that the charge recombination rates of the triarylamine–bithiophene–benzothiadiazole–cyanoacrylic acid dyes are strongly dependent on the structural modification at the acceptor unit: The insertion of a phenyl ring between the benzothiadiazole and cyanoacrylic acid units slows down the back electron transfer of the charge separated state by over five times [16]. This remarkable rate deceleration was attributed to the twisted structure at the phenylene bridge in the oxidized state of the D–$\pi$–A dye. Although we have no experimental data for rates of electron injection and charge recombination processes of the dyes on the $TiO_2$ surface, the DFT-optimized structures of the radical cations **7m**$^{+\bullet}$ and **12m**$^{+\bullet}$ show that the spatial distance between the N atom of the triarylamine unit and the carbonyl C atom of the anchoring group in **7m**$^{+\bullet}$ (23.8 Å) is shorter than that in **12m**$^{+\bullet}$ (25.7 Å). This indicates that the cation center of **12**$^{+\bullet}$ may be more separated than that of **7**$^{+\bullet}$ from the $TiO_2$ surface. Furthermore, the $\pi$ conjugation is somewhat interrupted at the phosphole–phenylene bridge both in the neutral state **12m** (dihedral angle = 43.2°) and in the radical cation **12m**$^{+\bullet}$ (dihedral angle = 42.6°). This is in marked contrast to the coplanar geometries at the phosphole–vinylene bridges of **7m** (dihedral angle = 7.2°) and **7m**$^{+\bullet}$ (dihedral angle = 8.3°). Accordingly, the charge recombination from the electrons in the CB to **12**$^{+\bullet}$ may be more retarded than that to **7**$^{+\bullet}$.

## CONCLUSIONS

In summary, we have synthesized a new class of D–$\pi$–A dyes composed of triarylamine (D), terthiophene ($\pi$), and phosphole (A) subunits, by using the titanacycle-mediated metathesis and Stille coupling reactions as the key steps. The new dyes displayed broad and split absorption bands in the visible region with the optical HOMO–LUMO gaps of 2.13–2.23 eV. The LC-TD-DFT calculations of the model compounds suggest that the observed $\pi$–$\pi^*$ transitions have the large CT character. With the N,S,P-hybrid dyes in hand, we prepared DSSCs and examined their cell performances for the first time. Under the optimized conditions, the new D–$\pi$–A dyes showed the power conversion efficiencies of up to 5.6%, which is the highest value ever reported for the phosphole-containing DSSCs. Although the collection of the NIR light has not been achieved yet, the present findings corroborate the potential utility of the phosphole skeletons as the acceptor components in the D–$\pi$–A sensitizers. Further studies on the construction of more $\pi$-extended N,S,P-hybrid dyes are now underway.

## EXPERIMENTAL

All melting points were recorded on a Yanagimoto micro melting point apparatus and are uncorrected. $^1$H and $^{13}$C{$^1$H} NMR spectra were recorded on a JEOL JNM-EX400 or AL300 spectrometer. Chemical shifts are reported in ppm as relative values versus tetramethylsilane ($^1$H and $^{13}$C) or phosphoric acid ($^{31}$P). High-resolution mass spectra (HRMS) were obtained on a Thermo Fisher Scientific Exactive spectrometer for atmosphere pressure chemical ionization (APCI) and electrospray ionization (ESI). UV–vis absorption and fluorescence spectra were measured on a PerkinElmer Lambda 900 UV/vis/NIR spectrometer and on a Horiba FluoroMax-3 spectrometer, respectively. 1-(Thiophene-2-yl)hepta-1,6-diyne [8a] and ethyl iodoacrylate [17] were prepared according to the reported procedures. THF was distilled from sodium benzophenone ketyl before use. Other chemicals and solvents were of reagent-grade quality and used without further purification unless otherwise noted. Thin-layer chromatography was performed with Alt. 5554 DC-Alufolien Kieselgel 60 F254 (Merck), and preparative column chromatography performed using UltraPure Silicagel (SiliCycle Inc) or Silica Gel 60 (Nacalai tesque). All reactions were performed under an argon atmosphere.

### *Compound* **1**

A mixture of 1-(thiophen-2-yl)hepta-1,6-diyne (5.0 g, 29 mmol), (*E*)-ethyl 3-iodoacrylate (6.547 g, 29.0 mmol), CuI (0.528 g, 2.77 mmol), *N,N*-dimethylglycine hydrochloride (1.185 g, 8.49 mmol), $Cs_2CO_3$ (26.928 g, 82.6 mmol), and 1,4-dioxane (70 mL) was stirred for 1.5 h at 80°C. The resulting mixture was then diluted with water and extracted with EtOAc three times. The combined organic extracts were washed with brine, dried over $Na_2SO_4$, and evaporated. The residue was subjected to silica gel column chromatography (hexane/EtOAc = 20/1). The fraction of $R_f$ = 0.33 was collected and evaporated to give **1** as a pale brown oil (6.670 g, 84%). $^1$H NMR (400 MHz, $CDCl_3$): $\delta$ 1.29 (t, $J$ = 7.1 Hz, 3H), 1.86 (quint, $J$ = 6.8 Hz, 2H), 2.56 (t, $J$ = 6.8 Hz, 4H), 4.20 (q, $J$ = 7.2 Hz, 2H), 6.16 (d, $J$ = 16.1 Hz, 1H), 6.75 (d, $J$ = 16.1 Hz, 1H), 6.94 (dd, $J$ = 3.9, 4.9 Hz, 1H), 7.13 (d, $J$ = 3.4 Hz, 1H), 7.18 (d, $J$ = 4.9 Hz, 1H); $^{13}$C{$^1$H} NMR (75 MHz, $CDCl_3$): $\delta$ 14.2, 18.9, 19.0, 27.3, 60.6, 74.6, 78.6, 92.8, 99.2, 123.8, 125.8, 126.1, 126.8, 129.7, 131.2, 166.0; IR (neat): $\nu_{max}$ 1714 cm$^{-1}$

(C=O); HRMS (APCI) *m/z*: Calcd for $C_{16}H_{16}O_2S$+H: 273.0944; Found 273.0942 ($[M + H]^+$).

### *Compound* **3**

To an $Et_2O$ solution (230 mL) containing **1** (4.00 g, 14.7 mmol) and Ti(O-*i*-Pr)$_4$ (4.4 mL, 14.7 mmol), *i*-PrMgCl (2.0 M, 14.7 mL, 29.4 mmol) was added at –70ºC and the mixture was stirred at –50°C. After 2.5 h, dichloro(phenyl)phosphine (2.0 mL, 14.7 mmol) was added to the solution and the resulting mixture was stirred for 1 h at 0°C and for 2 h at room temperature. A saturated aqueous $NH_4Cl$ solution was then added, and the mixture was filtered through a Celite bed. The organic layer was separated, and the aqueous phase was extracted with EtOAc three times. The combined organic extracts were washed with brine, dried over $Na_2SO_4$, and evaporated. The residue was recrystallized from MeOH at –78°C to give **3** as an orange solid (1.828 g, 33%). mp 115–117°C; $^1$H NMR (400 MHz, $CDCl_3$): $\delta$ 1.25 (t, $J$ = 7.1 Hz, 3H), 2.30–2.47 (m, 2H), 2.60–2.74 (m, 2H), 2.81–2.95 (m, 2H), 4.07–4.22 (m, 2H), 5.84 (d, $J$ = 15.1 Hz, 1H), 6.91 (t, $J$ = 4.4 Hz, 1H), 7.00 (d, $J$ = 3.4 Hz, 1H), 7.20 (d, $J$ = 4.9 Hz, 1H), 7.27–7.35 (m, 3H), 7.44 (td, $J$ = 2.0, 8.8 Hz, 2H), 7.55 (t, $J$ = 15.9 Hz, 1H); $^{13}$C{$^1$H} NMR (75 MHz, $CDCl_3$): $\delta$ 14.3, 27.8, 28.7, 29.2, 60.2, 116.8 (d, $J$ = 9.2 Hz), 125.6 (d, $J$ = 3.7 Hz), 125.7 (d, $J$ = 3.1 Hz), 127.7, 128.9 (d, $J$ = 8.6 Hz), 130.0 (d, $J$ = 1.9 Hz), 132.3 (d, $J$ = 12.3 Hz), 132.6 (d, $J$ = 2.5 Hz), 133.8 (d, $J$ = 20.3 Hz), 135.5, 138.4 (d, $J$ = 17.9 Hz), 139.8 (d, $J$ = 22.8 Hz), 152.6 (d, $J$ = 8.0 Hz), 165.1 (d, $J$ = 9.2 Hz), 167.4; $^{31}$P{$^1$H} NMR (162 MHz, $CDCl_3$): $\delta$ 28.6; IR (neat): $\nu_{max}$ 1704 cm$^{-1}$ (C=O); HRMS (APCI) *m/z*: Calcd for $C_{22}H_{21}O_2PS$ + H: 381.1073; Found 381.1072 ($[M + H]^+$).

### *Compound* **4**

To a solution of **3** (0.311 g, 0.82 mmol) in THF (20 mL), LDA (ca. 1.5 M, 0.63 mL, ca. 0.42 mmol) was added at –78ºC and the mixture was stirred for 2 h at the same temperature. Tributyltin chloride (0.31 mL, 1.2 mmol) was then added at –78°C, and the resulting mixture was gradually warmed to room temperature. After being stirred for 2 h at room temperature, the mixture was diluted with water and the aqueous phase was extracted with ether three times. The combined organic extracts were dried over anhydrous $Na_2SO_4$ and concentrated under reduced pressure to give **4** as a pale brown oil (0.757 g, ~100%). This compound was used without further purification in the subsequent reaction. $^1$H NMR ($CDCl_3$, 400 MHz): $\delta$ 0.86–1.66 (m, 30H), 2.35–2.41 (m, 2H), 2.62–2.74 (m, 2H), 2.74–2.90 (m, 2H), 4.09–4.19 (m, 2H), 5.82 (d, $J$ = 15.6 Hz, 1H), 6.96 (d, $J$ = 3.4 Hz, 1H), 7.11 (d, $J$ = 3.4 Hz, 1H), 7.17–7.30 (m, 3H), 7.46 (td, $J$ = 1.9, 7.3 Hz, 2H), 7.56 (t, $J$ = 15.6 Hz, 1H); $^{31}$P{$^1$H} NMR ($CDCl_3$, 162 MHz): $\delta$ 27.7; HRMS (ESI) *m/z*: Calcd for $C_{34}H_{47}O_2PSSn$ + H: 671.2129; Found 671.2140 ($[M + H]^+$).

### *Compound* **5**

To a solution of 4-((2,2'-bithiophen)-5-yl)-*N*,*N*-bis(4-(hexyloxy)phenyl)aniline (1.819 g, 2.98 mmol) in THF (50 mL), *N*-bromosuccinimide (0.547 g, 3.07 mmol) was added. The resulting mixture was stirred for 1.5 h at 0°C and 1.5 h at room temperature. Water was then added to the mixture, and the aqueous phase was extracted with $CH_2Cl_2$ five times. The combined organic extracts were dried over $Na_2SO_4$ and evaporated, and the residue was subjected to silica gel column chromatography (hexane/$CH_2Cl_2$ = 3:1). The fraction of $R_f$ = 0.35 was collected and evaporated to give **5** as a yellow oil (2.026 g, 99%). $^1$H NMR (400 MHz, DMSO-$d_6$): $\delta$ 0.88 (t, $J$ = 6.8 Hz, 6H), 1.24–1.32 (m, 8H), 1.40–1.41 (m, 4H), 1.66–1.73 (m, 4H), 3.94 (t, $J$ = 6.4 Hz, 4H), 6.75 (d, $J$ = 8.3 Hz, 2H), 6.91 (d, $J$ = 8.8 Hz, 4H), 7.03 (d, $J$ = 8.8 Hz, 4H), 7.13 (d, $J$ = 3.9 Hz, 1H), 7.21 (d, $J$ = 3.9 Hz, 1H), 7.28 (dd, $J$ = 3.4, 11.2 Hz, 2H), 7.46 (d, $J$ = 8.3 Hz, 2H); HRMS (ESI) *m/z*: Calcd for $C_{38}H_{42}BrNO_2S_2$: 687.1835; Found 687.1816 ($M^+$).

### *Compound* **6**

A mixture of **4** (296 mg), **5** (ca. 54 mg, ca. 0.078 mmol), Pd(PPh$_3$)$_4$ (34 mg, 0.029 mmol), and toluene (10 mL) was degassed by using a three-cycle freeze–pump–thaw sequence. The mixture was stirred for 24 h at 110°C, and water was then added. The aqueous phase was extracted with EtOAc three times, and the combined organic extracts were dried over $Na_2SO_4$ and evaporated. The residue was dissolved in $CH_2Cl_2$ (20 mL), followed by addition of $S_8$ (24 mg, 0.75 mmol). The resulting mixture was stirred for 2.5 h at room temperature and then subjected to silica gel column chromatography (hexane/EtOAc = 3:1). The reddish purple fraction of $R_f$ = 0.42 was collected and evaporated to give **6** as a reddish black solid (34 mg, 42%). $^1$H NMR ($CDCl_3$, 400 MHz): $\delta$ 0.87–0.94 (m, 6H), 1.23–1.37 (m, 11H), 1.43–1.46 (m, 4H), 1.74–1.81 (m, 4H), 2.36–2.40 (m, 2H), 2.85–2.93 (m, 4H), 3.93 (t, $J$ = 6.4 Hz, 4H), 4.12 (dd, $J$ = 6.8, 14.2 Hz, 2H), 6.22 (d, $J$ = 16.1 Hz, 1H), 6.83 (d, $J$ = 8.8 Hz, 4H), 6.90 (d, $J$ = 8.8 Hz, 2H), 7.00 (d, $J$ = 3.9 Hz, 1H), 7.03–7.09 (m, 8H), 7.32–7.52 (m,

7H), 7.88 (dd, $J$ = 6.8, 14.2 Hz, 2H); $^{31}P\{^1H\}$ NMR ($CDCl_3$, 162 MHz) $\delta$ 62.9; IR (neat): $\nu_{max}$ 1708 $cm^{-1}$ (C=O); HRMS (ESI) *m/z*: Calcd for $C_{60}H_{62}NO_4PS_4$: 1019.3294; Found 1019.3270 ($M^+$).

### *Compound* **7**

A mixture of **6** (112 mg, 0.11 mmol), $P(NMe_2)_3$ (0.15 mL, 0.83 mmol), and toluene (40 mL) was degassed by using a three-cycle freeze–pump–thaw sequence. The mixture was stirred for 5 h at 110°C. The conversion from the $\sigma^4$-P=S ester **6** to the $\sigma^3$-P ester was confirmed by TLC ($R_f$ = 0.65, hexane/EtOAc = 3:1). A mixture of the $\sigma^3$-P ester, aqueous NaOH solution (2 M, 0.7 mL, 1.4 mmol), THF (10 mL), and EtOH (10 mL) was degassed by using a three-cycle freeze–pump–thaw sequence. The resulting mixture was stirred for 24 h at 45°C, and 1 M aqueous HCl solution (1.4 mL) was then added. The aqueous phase was extracted with $CH_2Cl_2$ three times, and the combined organic extracts were dried over $Na_2SO_4$ and evaporated. The conversion from the $\sigma^3$-P ester to the $\sigma^3$-P carboxylic acid was confirmed only by TLC ($R_f$ = 0.33, hexane/EtOAc = 3:1). To a solution of the $\sigma^3$-P carboxylic acid in $CH_2Cl_2$ (20 mL), $S_8$ (48 mg, 1.5 mmol) was added. The resulting mixture was stirred for 16 h at room temperature and then subjected to silica gel column chromatography ($CH_2Cl_2$/acetone = 10:1). The reddish purple fraction of $R_f$ = 0.29 was collected and evaporated to give **7** as a reddish black solid (30 mg, 28%) after reprecipitation from hexane. mp 190–192°C; $^1H$ NMR ($CDCl_3$, 400 MHz): $\delta$ 0.89–0.93 (m, 6H), 1.32–1.81 (m, 16H), 2.37–2.41 (m, 2H), 2.84–2.90 (m, 2H), 2.90–2.97 (m, 2H), 3.93 (t, $J$ = 6.3 Hz, 4H), 6.21 (d, $J$ = 15.6 Hz, 1H), 6.83 (d, $J$ = 8.8 Hz, 4H), 6.90 (d, $J$ = 8.8 Hz, 2H), 7.01 (d, $J$ = 3.9 Hz, 1H), 7.04–7.10 (m, 8H), 7.32–7.52 (m, 7H), 7.87 (dd, $J$ = 7.3, 14.2 Hz, 2H). The OH proton of the carboxylic acid group was not clearly observed; $^{31}P\{^1H\}$ NMR ($CDCl_3$, 162 MHz) $\delta$ 62.8; IR (neat): $\nu_{max}$ 1669 $cm^{-1}$ (C=O); HRMS (ESI) *m/z*: Calcd for $C_{58}H_{58}NO_4PS_4$: 991.2981; Found 991.2959 ($M^+$).

### *Compound* **8**

A mixture of 1-(thiophen-2-yl)hepta-1,6-diyne (1.653 g, 6.95 mmol), ethyl 4-iodobenzoate (1.6 mL, 9.62 mmol), $PdCl_2(PPh_3)_2$ (201 mg, 0.29 mmol), CuI (31 mg, 0.16 mmol), triethylamine (7 mL), and toluene (21 mL) was stirred at room temperature. After 7 h, the suspension was treated with a saturated aqueous $NH_4Cl$ solution and extracted with $Et_2O$ twice. The combined organic extracts were washed with water, saturated aqueous $NaHCO_3$ solution, brine, dried over $Na_2SO_4$, and evaporated. The residue was subjected to silica gel column chromatography (hexane/EtOAc = 20:1). The fraction of $R_f$ = 0.20 was collected and evaporated to give **8** (1.541 g, 4.78 mmol, 69%) as a brown oil. $^1H$ NMR ($CDCl_3$, 300 MHz): $\delta$ 1.39 (t, $J$ = 7.1 Hz, 3H), 1.92 (t, $J$ = 7.0 Hz, 2H), 2.59–2.64 (m, 4H), 4.37 (q, $J$ = 7.0 Hz, 2H), 6.94 (dd, $J$ = 3.7, 5.1 Hz, 1H), 7.13 (d, $J$ = 3.7 Hz, 1H), 7.18 (d, $J$ = 5.1 Hz, 1H), 7.45 (d, $J$ = 8.4 Hz, 2H), 7.96 (d, $J$ = 8.4 Hz, 2H); $^{13}C\{^1H\}$ NMR (75 MHz, $CDCl_3$): $\delta$ 14.3, 18.8, 19.0, 27.6, 61.0, 74.5, 80.9, 92.4, 93.1, 123.9, 126.1, 126.8, 128.5, 129.4, 131.2, 131.5, 166.1. One of the $^{13}C$ peaks was not observed due to the peak overlapping; IR (neat): $\nu_{max}$ 1717 $cm^{-1}$ (C=O); HRMS (APCI) *m/z*: Calcd for $C_{20}H_{19}O_2S$: 323.1100; Found 323.1095 ($[M + H]^+$).

### *Compound* **9**

To an $Et_2O$ solution (80 mL) containing **8** (1.541 g, 4.78 mmol) and Ti(O-*i*-Pr)$_4$ (1.42 mL, 4.78 mmol), *i*-PrMgCl (2.0 M, 4.78 mL, 9.56 mmol) was added at −70ºC and the resulting mixture was stirred at −50ºC. After 2 h, dichloro(phenyl)phosphine (0.65 mL, 4.78 mmol) was added to the solution, and the resulting mixture was stirred for 1 h at 0°C and for 2 h at room temperature. A saturated aqueous $NH_4Cl$ solution was then added, and the mixture was filtered through a Celite bed. The organic layer was separated, and the aqueous phase was extracted with EtOAc three times. The combined organic extracts were washed with brine, dried over $Na_2SO_4$, and evaporated. The residue was recrystallized from MeOH at –78°C to give **9** (1.184 g, 58%) as an orange solid. mp 134–136°C; $^1H$ NMR (400 MHz, $CDCl_3$): $\delta$ 1.36 (t, $J$ = 7.1 Hz, 3H), 2.38–2.48 (m, 2H), 2.74–3.07 (m, 4H), 4.30–4.36 (m, 2H), 6.93 (m, 1H), 7.00 (m, 1H), 7.19 (d, $J$ = 4.9 Hz, 1H), 7.21–7.26 (m, 3H), 7.42–7.46 (m, 2H), 7.50 (d, $J$ = 7.8 Hz, 2H), 7.92 (d, $J$ = 8.3 Hz, 2H); $^{13}C\{^1H\}$ NMR (75 MHz, $CDCl_3$): $\delta$ 14.4, 23.4, 26.4, 29.0 (d, $J$ = 1.2 Hz), 29.6 (d, $J$ = 3.1 Hz), 32.2, 124.8 (d, $J$ = 5.5 Hz), 124.9 (d, $J$ = 15.4 Hz), 127.1 (d, $J$ = 10.5 Hz), 127.7 (d, $J$ = 4.3 Hz), 128.8 (d, $J$ = 8.6 Hz), 129.7 (d, $J$ = 1.2 Hz), 129.8 (d, $J$ = 1.2 Hz), 132.5 (d, $J$ = 14.8 Hz), 133.6 (d, $J$ = 19.7 Hz), 135.4 (d, $J$ = 24.0 Hz), 140.0 (d, $J$ = 23.4 Hz), 141.2 (d, $J$ = 19.1 Hz), 153.9 (d, $J$ = 9.2 Hz), 156.9 (d, $J$ = 9.9 Hz), 166.5; $^{31}P\{^1H\}$ NMR ($CDCl_3$, 162 MHz): $\delta$ 34.2; IR (neat): $\nu_{max}$ 1713 $cm^{-1}$ (C=O); HRMS (APCI) *m/z*: Calcd for $C_{26}H_{24}O_2PS$: 431.1229; Found 431.1223 ($[M + H]^+$).

### *Compound* **10**

To a solution of **9** (0.327 g, 0.76 mmol) in THF (15 mL), LDA (ca. 1.5 M, 0.76 mL, ca. 1.14 mmol) was added at –78°C and the mixture was stirred for 2 h at the same temperature. Tributyltin chloride (0.31 mL, 1.14 mmol) was then added, and the resulting mixture was stirred for 0.5 h at –78°C and 2 h at room temperature. The mixture was diluted with water, and the aqueous phase was extracted with ether three times. The combined organic extracts were dried over anhydrous $Na_2SO_4$ and concentrated under reduced pressure to give **10** as a brown oil (~100%). This compound was used without further purification in the subsequent reaction. $^1$H NMR ($CDCl_3$, 400 MHz): $\delta$ 0.87–1.61 (m, 30H), 2.40–2.44 (m, 2H), 2.78–3.07 (m, 4H), 4.33 (q, $J$ = 7.3 Hz, 2H), 6.99 (d, $J$ = 3.4 Hz, 1H), 7.12 (d, $J$ = 3.4 Hz, 1H), 7.19–7.22 (m, 3H), 7.46 (td, $J$ = 2.0, 7.8 Hz, 2H), 7.50 (d, $J$ = 7.8 Hz, 2H), 7.91 (d, $J$ = 8.3 Hz, 2H); $^{31}$P{$^1$H} NMR ($CDCl_3$, 162 MHz): $\delta$ 34.5; IR (neat): $\nu_{max}$ 1716 cm$^{-1}$ (C=O); HRMS (ESI) *m/z*: Calcd for $C_{38}H_{50}O_2PSSn$: 721.2286; Found 721.2345 ([M + H]$^+$).

### *Compound* **11**

A mixture of **10** (ca. 0.76 mmol), **7** (ca. 0.197 g, ca. 0.29 mmol), and $Pd(PPh_3)_4$ (93 mg, 0.080 mmol), and toluene (30 mL) was degassed by using a three-cycle freeze–pump–thaw sequence. The resulting mixture was stirred for 23 h at 110°C, and water was then added. The aqueous phase was extracted with EtOAc three times, and the combined organic extracts were dried over $Na_2SO_4$ and evaporated. The residue was dissolved in $CH_2Cl_2$ (70 mL), followed by addition of $S_8$ (120 mg, 3.7 mmol). The resulting mixture was stirred for 3 h at room temperature and then subjected to silica gel column chromatography (hexane/EtOAc = 3:1). The reddish purple fraction of $R_f$ = 0.39 was collected and evaporated to give **11** as a reddish black solid (0.115 g, 38%). $^1$H NMR (400 MHz, $CDCl_3$): $\delta$ 0.87–0.94 (m, 6H), 1.33–1.39 (m, 11H), 1.43–1.48 (m, 4H), 1.74–1.81 (m, 4H), 2.40 (m, 2H), 2.95 (m, 2H), 3.02 (m, 2H), 3.93 (t, $J$ = 6.8 Hz, 4H), 4.33 (q, $J$ = 7.3 Hz, 2H), 6.83 (d, $J$ = 8.8 Hz, 4H), 6.90 (d, $J$ = 8.8 Hz, 2H), 7.01 (d, $J$ = 3.9 Hz, 1H), 7.03–7.09 (m, 4H), 7.05 (d, $J$ = 8.8 Hz, 4H), 7.28 (d, $J$ = 3.9 Hz, 1H), 7.37 (d, $J$ = 8.8 Hz, 2H), 7.42–7.53 (m, 3H), 7.64 (d, $J$ = 8.8 Hz, 2H), 7.93 (d, $J$ = 8.3 Hz, 2H), 7.93 (dd, $J$ = 6.8, 15.2 Hz, 2H); $^{31}$P{$^1$H} NMR ($CDCl_3$, 162 MHz): $\delta$ 66.8; IR (neat): $\nu_{max}$ 1716 cm$^{-1}$ (C=O); HRMS (ESI) *m/z*: Calcd for $C_{64}H_{64}NO_4PS_4$: 1069.3450; Found 1069.3429 (M$^+$).

### *Compound* **12**

A mixture of **11** (89 mg, 0.083 mmol), $P(NMe_2)_3$ (0.17 mL, 0.94 mmol), and toluene (40 mL) was degassed by using a three-cycle freeze–pump–thaw sequence. The resulting mixture was stirred for 1 h at 110°C, and the conversion from the $\sigma^4$-P=S ester **11** to the $\sigma^3$-P ester was confirmed by TLC ($R_f$ = 0.62, hexane/EtOAc = 3:1). A mixture of the $\sigma^3$-P ester, aqueous NaOH solution (2 M, 1.0 mL, 2.0 mmol), THF (10 mL), and EtOH (10 mL) was degassed by using a three-cycle freeze–pump–thaw sequence. The resulting mixture was stirred for 20 h at 45°C, and 1 M aqueous HCl solution (2.0 mL) was then added. The aqueous phase was extracted with $CH_2Cl_2$ three times, and the combined organic extracts were dried over $Na_2SO_4$ and evaporated. The conversion from the $\sigma^3$-P ester to the $\sigma^3$-P carboxylic acid was confirmed only by TLC ($R_f$ = 0.21, hexane/EtOAc = 3:1). To a solution of the $\sigma^3$-P carboxylic acid in $CH_2Cl_2$ (30 mL), $S_8$ (246 mg, 7.7 mmol) was added. The resulting mixture was stirred for 25 h at 40°C and then subjected to silica gel column chromatography ($CH_2Cl_2$/acetone = 10:1). The red fraction of $R_f$ = 0.13 was collected and evaporated to give **12** as a reddish black solid (51 mg, 59%) after reprecipitation from hexane. mp 256–258°C; $^1$H NMR (400 MHz, $CDCl_3$): $\delta$ 0.88–0.93 (m, 6H), 1.34–1.38 (m, 8H), 1.43–1.46 (m, 4H), 1.74–1.81 (m, 4H), 2.42 (m, 2H), 2.97 (m, 2H), 3.04 (m, 2H), 3.93 (t, $J$ = 6.6 Hz, 4H), 6.83 (d, $J$ = 8.8 Hz, 4H), 6.91 (m, 2H), 7.01 (d, $J$ = 4.4 Hz, 1H), 7.05–7.09 (m, 8H), 7.29 (d, $J$ = 4.4 Hz, 1H), 7.37 (d, $J$ = 8.8 Hz, 2H), 7.43–7.55 (m, 3H), 7.67 (d, $J$ = 8.3 Hz, 2H), 7.94 (dd, $J$ = 7.3, 14.2 Hz, 2H), 7.97 (d, $J$ = 8.3 Hz, 2H). The OH proton of the carboxylic acid group was not clearly observed; $^{31}$P{$^1$H} NMR ($CDCl_3$, 162 MHz): $\delta$ 66.7; IR (neat): $\nu_{max}$ 1683 cm$^{-1}$ (C=O); HRMS (APCI) *m/z*: Calcd for $C_{62}H_{60}NO_4PS_4$: 1041.3137; Found 1041.3113 (M$^+$).

### *Electrochemical Measurements*

Electrochemical measurements of **3**, **7**, **9**, and **12** were performed at room temperature on a CH Instruments model 660A electrochemical workstation using a glassy carbon working electrode, a platinum wire counterelectrode, and an Ag/Ag$^+$ [0.01 M $AgNO_3$, 0.1 M $Bu_4NPF_6$ (MeCN)] reference electrode. The potentials were calibrated with Fc/Fc$^+$. The observed voltammograms (scan rate = 60 mV s$^{-1}$) are summarized in Fig. 7.

### *Computational Details*

The geometries of **7m**, **12m**, **7m**$^{+\bullet}$, and **12m**$^{+\bullet}$ were optimized using the DFT method with the

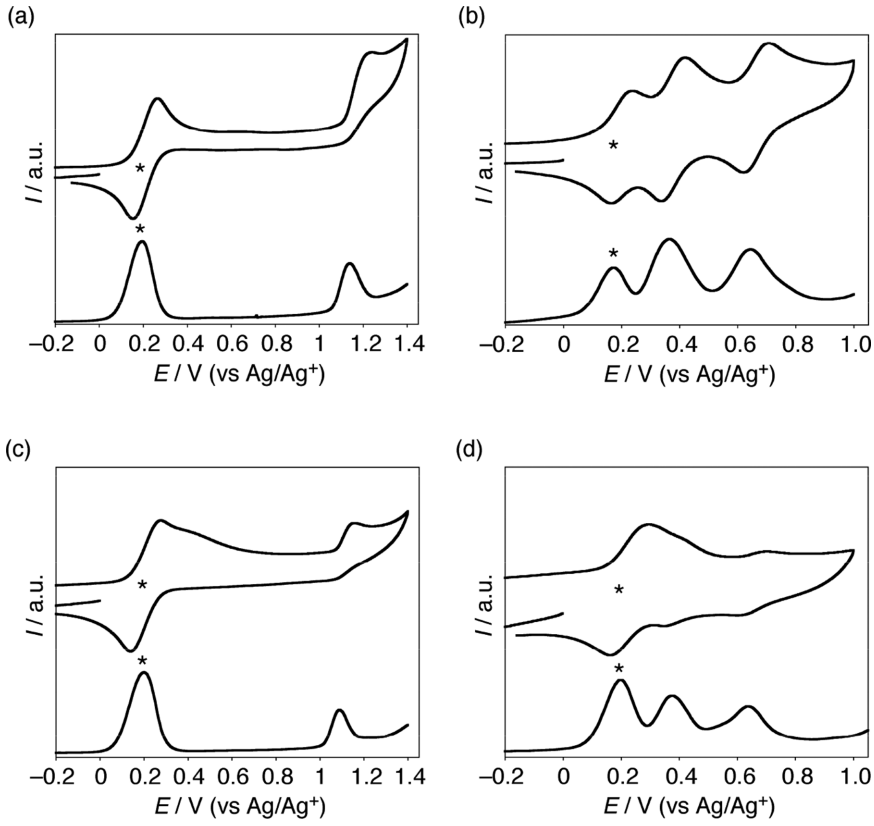


**FIGURE 7** Cyclic voltammograms (upper) and differential pulse voltammograms (lower) for (a) **3**, (b) **7**, (c) **9**, and (d) **12**. The asterisks indicate a $Fc/Fc^+$ couple.

6-31G(d,p) basis set [18] for all atoms. The functional of DFT was the Becke, three-parameter, Lee–Yang–Parr (B3LYP) exchange-correlation functional [19], in which the solvent effect of toluene was included by the polarizable continuum model (PCM) method [20]. We confirmed that the optimized geometries were not in saddle but in stable points. The excitation energies and oscillator strengths listed in Table 2 were computed with the TD-DFT method with the 6-31++G(d,p) basis set [18, 21], in which the solvent effect of toluene was included by the PCM method [20]. The functional of TD-DFT was the LC-BLYP exchange-correlation functional [22]. All the calculations were carried out using the Gaussian 09 suite of programs [23]. Selected molecular orbitals and their energies of **7m** and **12m** are summarized in Fig. 2.

### *Fabrication of the Dye-Sensitized $TiO_2$ Electrode*

The preparation of $TiO_2$ electrodes and the fabrication of sealed cells for photovoltaic measurements were performed following the previously reported method [13, 24]. The details of this work were described as follows.

Nanocrystalline $TiO_2$ particles ($d = 20$ nm, CCIC: PST23NR, JGC-CCIC) were used as the transparent layer of the photoanode, whereas submicrocrystalline $TiO_2$ particles ($d = 400$ nm, CCIC:PST400C, JGC-CCIC) as the light-scattering layers of the photoanode. The working electrode was prepared by cleaning a fluorine-doped tin oxide (FTO) glass (solar 4 mm thickness, 10 Ω/o, Nippon Sheet Glass) with a detergent solution in an ultrasonic bath for 15 min, rinsing with distilled water, ethanol, and air-drying. The electrode was subjected to UV-$O_3$ irradiation for 18 min, immersed into a solution of freshly prepared 40 mM aqueous $TiCl_4$ at 70°C for 30 min, washed with distilled water, ethanol, and dried. Nanocrystalline $TiO_2$ paste was coated onto the FTO glass by screen printing, followed by standing in a clean box for a few minutes and dried at 125°C for 6 min, repeating to attain a final thickness of 12 $\mu$m (12 $\mu$m thickness of the PST23NR $TiO_2$ layer). A layer of 4 $\mu$m submicrocrystalline $TiO_2$ paste was deposited in the same fashion as the nanocrystalline layer. Finally, the electrode was heated under an airflow at 325°C for 5 min, at 375°C for 5 min, at 450°C for 15 min, and at 500°C for 15 min. The thickness of the films was determined

using a surface profiler (Surfcom 130A, Accretech). The size of the $TiO_2$ film was 0.16 $cm^2$ (4 × 4 mm). The $TiO_2$ electrode was then subjected to immersion into a solution of freshly prepared 40 mM aqueous $TiCl_4$ at 70°C for 25 min before rinsing with distilled water and ethanol, and air-drying. The electrode was sintered at 500°C for 30 min, cooled to 70°C, and immersed into the dye solution at 25°C in the dark for the prescribed times. The $TiO_2$ electrode was immersed into a toluene solution of 0.30 mM phosphole dye. The $TiO_2$ electrode stained with phosphole dye is denoted as a $TiO_2$/phosphole dye.

The counterelectrode was prepared by drilling a small hole in an FTO glass, rinsing with distilled water and ethanol before treatment with 0.1 M HCl/2-propanol in an ultrasonic bath for 15 min. After heating in air at 400°C for 15 min, platinum was deposited by coating the electrode with a solution of $H_2PtCl_6$ (2 mg in 1 mL ethanol) twice and heating in air at 400°C for 15 min.

The sandwich cell was prepared by using the dye-anchored $TiO_2$ film as a working electrode and a counter Pt electrode, which were assembled with a hotmelt-ionomer film of Surlyn polymer gasket (DuPont), and the superimposed electrodes were tightly held and heated at 110°C to seal the two electrodes. The aperture of the Surlyn frame was larger by 2 mm than that of the area of the $TiO_2$ film, and its width was 1 mm. The hole in the counterelectrode was sealed by a film of Surlyn. A hole was then made in the film of Surlyn covered on the hole by a needle. A drop of an electrolyte was put on the hole in the back of the counterelectrode. It was introduced into the cell via vacuum backfilling. Finally, the hole was sealed using the Surlyn film and a cover glass (0.13–0.17 mm thickness). A solder was applied on each edge of the FTO electrodes. An electrolyte solution used was 1.0 M 1,3-dimethylimidazolium iodide, 0.06 M $I_2$, 0.05 M LiI, 0.1 M guanidinium thiocyanate, and 0.50 M 4-*tert*-butylpyridine in acetonitrile.

IPCE and photocurrent-voltage (*J*–*V*) performance were measured on an action spectrum measurement setup (CEP-2000RR, Bunkoukeiki) and a solar simulator (PEC-L10, Peccell Technologies) with a simulated sunlight of AM 1.5 (100 mW $cm^{-2}$), respectively: IPCE (%) = 100 × 1240 × $i/(W_{in} \times \lambda)$, where $i$ is the photocurrent density (A $cm^{-2}$), $W_{in}$ is the incident light intensity (W $cm^{-2}$), and $\lambda$ is the excitation wavelength (nm). During the photovoltaic measurements, a black plastic mask was attached on the back of the $TiO_2$ electrode except for the $TiO_2$ film region to reduce scattering light.

## *REFERENCES*


[1] (a) O'Regan, B.; Grätzel, M. Nature 1991, 353, 737; (b) Nazeeruddin, M. K.; Kay, A.; Rodicio, I.; Humphry-Baker, R.; Müller, E.; Liska, P.; Vlachopoulos, N.; Grätzel, M. J Am Chem Soc 1993, 115, 6382.

[2] For selected reviews, see: (a) Hagfeldt, A.; Grätzel, M. Chem Rev 1995, 95, 49; (b) Wang, P.; Zakeeruddin, S. M.; Moser, J. E.; Nazeeruddin, M. K.; Sekiguchi, T.; Grätzel, M. Nat Mater 2003, 2, 402; (c) Hagfeldt, A.; Grätzel, M. Acc Chem Res 2000, 33, 269; (d) Islam, A.; Sugihara, H.; Arakawa, H. J Photochem Photobiol A 2003, 158, 131; (e) Nazeeruddin, M. K. (Ed.): Coord Chem Rev 2004, 248 (special issue for DSSC); (f) Grätzel, M. Acc Chem Res 2009, 42, 1788; (g) Hagfeldt, A.; Boschloo, G.; Sun, L.; Kloo, L.; Pettersson, H. Chem Rev 2010, 110, 6595; (h) Reynal, A.; Palomares, E. Eur J Inorg Chem 2011, 4509; (i) Listorti, A.; O'Regan, B.; Durrant, J. R. Chem Mater 2011, 23, 3381; (j) Yin, J.-F.; Velayudham, M.; Bhattacharya, D.; Lin, H.-C.; Lu, K.-L. Coord Chem Rev 2012, 256, 3008; (k) Robson, K. C. D.; Bomben, P. G.; Berlinguette, C. P. Dalton Trans 2012, 41, 7814; (l) Hardin, B. E.; Snaith, H. J.; McGehee, M. D. Nature Photon 2012, 6, 162; (m) Bozic-Weber, B.; Constable, E. C.; Housecroft, C. E. Coord Chem Rev 2013, 257, 3089.

[3] For recent reviews, see: (a) Mishra, A.; Fischer, M. K. R.; Bäuerle, P. Angew Chem, Int Ed 2009, 48, 2474; (b) Ooyama, Y.; Harima, Y. Eur J Org Chem 2009, 2903; (c) Imahori, H.; Umeyama, T.; Ito, S. Acc Chem Res 2009, 42, 1809; (d) Imahori, H.; Umeyama, T.; Kurotobi, K.; Takano, Y. Chem Commun 2012, 48, 4032; (e) Ning, Z.; Fu, Y.; Tian, H. Energy Environ Sci 2010, 3, 1170; (f) Ooyama, Y.; Harima, Y. ChemPhysChem 2012, 13, 4032; (g) Yin, Q. S.; Li, H. J.; He, T. Sci China A 2012, 55, 677; (h) Clifford, J. N.; Planells, M.; Palomares, E. J Mater Chem 2012, 22, 24195; (i) Wu, Y.; Zhu, W. Chem Soc Rev 2013, 42, 2039; (j) Liang, M.; Chen, J. Chem Soc Rev 2013, 42, 3453; (k) Ahmad, S.; Guillén, E.; Kavan, L.; Grätzel, M.; Nazeeruddin, M. K. Energy Environ Sci 2013, 6, 3439; (l) Li, L.-L.; Diau, E. W.-G. Chem Soc Rev 2013, 42, 291; (m) Mathew, S.; Yella, A.; Gao, P.; Humphry-Baker, R.; Curchod, B. F. E.; Ashari-Astani, N.; Tavernelli, I.; Rothlisberger, U.; Nazeeruddin, Md. K.; Grätzel, M. Nature Chem 2014, 6, 242; (n) Joly, D.; Pellejà, L.; Narbey, S.; Oswald, F.; Chiron, J.; Clifford, J. N.; Palomares, E.; Demadrille, R. Sci Rep 2013, 4, 4033.

[4] For example, see: (a) Koumura, N.; Wang, Z.-S.; Mori, S.; Miyashita, M.; Suzuki, E.; Hara, K. J Am Chem Soc 2006, 128, 14256 (addition and correction, 2008, 130, 4202); (b) Kim, S.; Lee, J. K.; Kang, S. O.; Ko, J.; Yum, J.-H.; Fantacci, S.; De Angelis, F.; Di Censo, D.; Nazeeruddin, M. K.; Grätsel, M. J Am Chem Soc 2006, 128, 16701; (c) Hagberg, D. P.; Marinado, T.; Karlsson, K. M.; Nonomura, K.; Qin, P.; Boschloo, G.; Brinck, T.; Hagfeldt, A.; Sun, L. J Org Chem 2007, 72, 9550; (d) Wang, Z.-S.; Koumura, N.; Cui, Y.; Takahashi, M.; Sekiguchi, H.; Mori, A.; Kubo, T.; Furube, A.; Hara, K. Chem Mater 2008, 20, 3993; (e) Yum, J.-H.; Hagberg, D. P.; Moon, S.-J.; Karlsson, K. M.; Marinado, T.; Sun, L.; Hagfeldt, A.; Nazeeruddin, M. K.; Grätsel, M. Angew Chem, Int Ed 2009, 48, 1576;

(f) Zhang, G.; Bala, H.; Cheng, Y.; Shi, D.; Lv, X.; Yu, Q.; Wang, P. Chem Commun 2009, 2198; (g) Koumura, N.; Wang, Z.-S.; Miyashita, M.; Sekiguchi, H.; Cui, Y.; Mori, A.; Mori, S.; Hara, K. J Mater Chem 2009, 19, 4829; (h) Zeng, W.; Cao, Y.; Bai, Y.; Wang, Y.; Shi, Y.; Zhang, M.; Wang, F.; Pan, C.; Wang, P. Chem Mater 2010, 22, 1915; (i) Ren, X.; Jiang, S.; Cha, M.; Zhou, G.; Wang, Z.-S. Chem Mater 2012, 24, 3493.

[5] For recent reviews on $\pi$-conjugated phospholes, see (a) Mathey, F. Angew Chem, Int Ed 2003, 42, 1578; (b) Hissler, M.; Dyer, P. W.; Réau, R. Top Curr Chem 2005, 250, 127; (c) Hissler, M.; Dyer, P. W.; Réau, R. Coord Chem Rev 2003, 244, 1; (d) Baumgartner, T.; Réau, R. Chem Rev 2006, 106, 4681 (correction 2007, 107, 303); (e) Hobbs, M. G.; Baumgartner, T. Eur J Inorg Chem 2007, 3611; (f) Réau, R.; Dyer, P. W. In Comprehensive Heterocyclic Chemistry III; Ramsden, C. A., Scriven, E. F. V., Taylor, R. J. K., Eds.; Elsvier: Oxford, UK, 2008; Ch. 3.15, pp. 1029–1048; (g) Hissler, M.; Lescop, C.; Réau, R. C R Chim 2008, 11, 628; (h) Nyulászi, L.; Benkő, Z. Top Heterocycl Chem 2009, 19, 27; (i) Matano, Y.; Imahori, H. Org Biomol Chem 2009, 7, 1258; (j) Ren, Y.; Baumgartner, T. Dalton Trans 2012, 41, 7792.

[6] (a) Tsuji, H.; Sato, K.; Sato, Y.; Nakamura, E. J Mater Chem 2009, 19, 3364; (b) Matano, Y.; Saito, A.; Fukushima, T.; Tokudome, Y.; Suzuki, F.; Sakamaki, D.; Kaji, H.; Ito, A.; Tanaka, K.; Imahori, H. Angew Chem, Int Ed 2011, 50, 8016.

[7] (a) Matano, Y.; Miyajima, T.; Nakabuchi, T.; Matsutani, Y.; Imahori, H. J Org Chem 2006, 71, 5792; (b) Matano, Y.; Nakashima, M.; Saito, A.; Imahori, H. Org Lett 2009, 11, 3338; (c) Matano, Y.; Fujita, M.; Saito, A.; Imahori, H. C R Chim 2010, 13, 1035; (d) Saito, A.; Matano, Y.; Imahori, H. Org Lett 2010, 12, 2675; (e) Matano, Y.; Kon, Y.; Saito, A.; Kimura, Y.; Murafuji, T.; Imahori, H. Chem Lett 2011, 40, 919; (f) Matano, Y.; Saito, A.; Fujita, M.; Imahori, H. Heteroatom Chem 2011, 22, 457; (g) Hayashi, Y.; Matano, Y.; Suda, K.; Kimura, Y.; Nakao, Y.; Imahori, H. Chem Eur J 2012, 18, 15972; (h) Matano, Y.; Ohkubo, H.; Honsho, Y.; Saito, A.; Seki, S.; Imahori, H. Org Lett 2013, 15, 932; (i) Matano, Y.; Ohkubo, H.; Miyata, T.; Watanabe, Y.; Hayashi, Y.; Umeyama, T.; Imahori, H. Eur J Inorg Chem 2014, 2014, 1620.

[8] (a) Matano, Y.; Miyajima, T.; Imahori, H.; Kimura, Y. J Org Chem 2007, 72, 6200; (b) Matano, Y.; Hayashi, Y.; Suda, K.; Kimura,Y.; Imahori, H. Org Lett 2013, 15, 4458.

[9] Matano, Y.; Nakashima, M.; Imahori, H. Angew Chem, Int Ed 2009, 48, 4002.

[10] Matano, Y.; Imahori, H. J Synth Org Chem Jpn 2011, 70, 629.

[11] Kira, A.; Shibano, Y.; Kang, S.; Hayashi, H.; Umeyama, T.; Matano, Y.; Imahori, H. Chem Lett 2010, 39, 448.

[12] (a) Sato, F.; Urabe, H.; Okamoto, S. Pure Appl Chem 1999, 71, 1511; (b) Sato, F.; Urabe, H.; Okamoto, S. Chem Rev 2000, 100, 2835.

[13] Kurotobi, K.; Toude, Y.; Kawamoto, K.; Fujimori, Y.; Ito, S.; Chabera, P.; Sundström, V.; Imahori, H. Chem Eur J 2013, 19, 17075.

[14] Hara, K.; Sato, T.; Katoh, R.; Furube, A.; Ohga, Y.; Shipo, A.; Suga, S.; Sayama, K.; Sugihara, H.; Arakawa, H. J Phys Chem B 2003, 107, 597.

[15] (a) Clifford, J. N.; Palomares, E.; Nazeeruddin, M. K.; Grätzel, M.; Nelson, J.; Li, X.; Long, N. J.; Durrant, J. R. J Am Chem Soc 2004, 126, 5225; (b) Imahori, H.; Kang, S.; Hayashi, H.; Haruta, M.; Kurata, H.; Isoda, S.; Canton, S, E.; Infahsaeng, Y.; Kathiravan, A.; Pacher, T.; Chabera, P.; Yartsev, A. P.; Sundström, V. J Phys Chem A 2011, 115, 3679; (c) Ye, S.; Kathiravan, A.; Hayashi, H.; Tong, Y.; Infahsaeng, Y.; Chabera, P.; Pascher, T.; Yartsev, A. P.; Isoda, S. Imahori, H.; Sundström, V. J Phys Chem C 2013, 117, 6066.

[16] Haid, S.; Marszalek, M.; Mishra, A.; Wielopolski, M.; Teuscher, J.; Moser, J.-E.; Humphry-Baker, R.; Zakeeruddin, S. M.; Grätzel, M.; Bäuerle, P. Adv Funct Mater 2012, 22, 1291.

[17] Chen, F.; Zhang, X. Chem Lett 2011, 40, 978.

[18] (a) Ditchfield, R.; Hehre, W. J.; Pople, J. A. J Chem Phys 1971, 54, 724; (b) Hehre, W. J.; Ditchfield, R.; Pople, J. A. J Chem Phys 1972, 56, 2257; (c) Hariharan, P. C.; Pople, J. A. Theor Chim Acta 1972, 28, 213; (d) Francl, M. M.; Pietro, W. J.; Hehre, W. J.; Binkley, J. S.; Gordon, M. S.; DeFrees, D. J.; Pople, J. A. J Chem Phys 1982, 77, 3654.

[19] (a) Becke, A. D. J Chem Phys 1988, 98, 5648; (b) Lee, C.; Yang, W.; Parr, R. G. Phys Rev B 1988, 37, 785.

[20] Cancès, M. T.; Mennucci, B.; Tomasi, J. J Chem Phys 1997, 107, 3032.

[21] Clark, T.; Chandrasekhar, J.; Spitznagel, G. W.; Schleyer, P. von R. J Comput Chem 1983, 4, 294.

[22] Tawada, Y.; Tsuneda, T.; Yanagisawa, S.; Yanai, T.; Hirao, K. J Chem Phys 2004, 120, 8425.

[23] Frisch, M. J.; Trucks, G. W.; Schlegel, H. B.; Scuseria, G. E.; Robb, M. A.; Cheeseman, J. R.; Scalmani, G.; Barone, V.; Mennucci, B.; Petersson, G. A.; Nakatsuji, H.; Caricato, M.; Li, X.; Hratchian, H. P.; Izmaylov, A. F.; Bloino, J.; Zheng, G.; Sonnenberg, J. L.; Hada, M.; Ehara, M.; Toyota, K.; Fukuda, R.; Hasegawa, J.; Ishida, M.; Nakajima, T.; Honda, Y.; Kitao, O.; Nakai, H.; Vreven, T.; Montgomery, J. A., Jr.; Peralta, J. E.; Ogliaro, F.; Bearpark, M.; Heyd, J. J.; Brothers, E.; Kudin, K. N.; Staroverov, V. N.; Keith, T.; Kobayashi, R.; Normand, J.; Raghavachari, K.; Rendell, A.; Burant, J. C.; Iyengar, S. S.; Tomasi, J.; Cossi, M.; Rega, N.; Millam, J. M.; Klene, M.; Knox, J. E.; Cross, J. B.; Bakken, V.; Adamo, C.; Jaramillo, J.; Gomperts, R.; Stratmann, R. E.; Yazyev, O.; Austin, A. J.; Cammi, R.; Pomelli, C.; Ochterski, J. W.; Martin, R. L.; Morokuma, K.; Zakrzewski, V. G.; Voth, G. A.; Salvador, P.; Dannenberg, J. J.; Dapprich, S.; Daniels, A. D.; Farkas, O.; Foresman, J. B.; Ortiz, J. V.; Cioslowski, J.; Fox, D. J. Gaussian 09, Revision C.01; Gaussian, Wallingford CT, 2010.

[24] (a) Imahori, H.; Matsubara, Y.; Iijima, H.; Umeyama, T.; Matano, Y.; Ito, S.; Niemi, M.; Tkachenko, N. V.; Lemmetyinen, H. J Phys Chem C 2010, 114, 10656; (b) Ito, S.; Murakami, T.; Comte, P.; Liska, P.; Grätzel, C.; Nazeeruddin, M. K.; Grätzel, M. Thin Solid Films 2008, 516, 4613.